Comparison of illumination analyses using one-way and full-wave propagators

Mingqiu Luo, Jun Cao, Xiaobi Xie, and Ru-Shan Wu
Modeling and Imaging Laboratory, Institute of Geophysics and Planetary Physics, University of California, Santa Cruz, CA, 95064, USA

Summary

In this paper, we compare one-way wave propagator and full-wave propagator such as finite difference (FD) method in the evaluation of illumination and acquisition dip response (ADR) maps. For the case of 2D SEG/EAGE salt model, the illumination and ADR maps by the one-way method and the FD method have similar general distributions in space and angle domain. However, some difference exists in absolute values, especially for the subsalt area. This is due to the strong effects of transmission loss caused by salt boundary scattering, reflection and defocusing. The difference in wide-angle amplitude behavior is also noticeable. Therefore, in most cases illumination analysis calculated by one-way wave propagators can provide reliable evaluation.

Introduction

Illumination analysis in the target area is a powerful tool to study the influences of acquisition aperture and overlaying structure to the quality of image. Most existing techniques for predicting illumination intensity distributions under certain acquisition geometries are based on ray tracing modeling (Berkhout, 1997; Muerdter et al., 2001a, 2001b, 20001c; Schneider, 1999; Bear et al., 2000). Although ray tracing is inexpensive, the resulting illumination map may bear large errors in complex areas due to the high frequency approximation involved and the singularity problem of ray tracing. This may severely limit its accuracy (Hoffmann, 2001).

Recently, techniques to obtain the localized angle domain information for the frequency domain wave field based on beamlet decomposition have been developed (Wu et al., 2000) and applied to directional illumination analysis (Wu and Chen, 2002, 2003). Direct local plane wave decomposition can be also used for this purpose (Xie and Wu, 2002). Based on these techniques, one-way wave propagators, including the GDF (Gabor-Daubechies Frame) beamlet propagator, the local cosine (LCB) beamlet propagator (Wang and Wu, 2002; Luo and Wu, 2003) and generalized screen propagator (GSP), FFD, among others, can be applied calculate the illumination maps for a given acquisition geometry and velocity model.

Compared to the ray tracing method, the one-way wave propagator can provide more accurate wave field for complex model. But for the one-way method, the effects of transmission loss, multiple scattering, have been neglected and wide-angle amplitude approximation is involved. In order to understand and evaluate these effects, we apply the full-wave Finite Difference (FD) method to the calculation of illumination maps, and compare the results with those generated by a one-way propagator, here the LCB beamlet method. Finally we discuss the influence of using one-way wave propagators to the quality of illumination mapping.

Angle-domain illumination analysis

According to the angle decomposition techniques, the wave field decomposed into beamlets which can be considered as local plane waves centered at the special location. For a given acquisition geometry, the frequency-space domain Green's function from source s to subsurface point $\vec{x}$ can be decomposed at the image region to a summation of all angle components. That is,

$$G(s,\vec{x},\omega)=\sum_{\theta_s} G(s,\vec{x},\theta_s,\omega) \qquad (1)$$

where $G(s,\vec{x},\omega)$ is the space-domain Green's function and $G(s,\vec{x},\theta_s,\omega)$ is its angle-component at θ_s. Similarly, the frequency-space domain Green's function from subsurface point $\vec{x}$ to receiver r can be decomposed to

$$G(\vec{x},r,\omega)=\sum_{\theta_g} G(\vec{x},\theta_g,r,\omega) \qquad (2)$$

where $G(\vec{x},r,\omega)$ is the frequency-space domain Green's function and $G(\vec{x},\theta_g,r,\omega)$ is its component in angle θ_g.

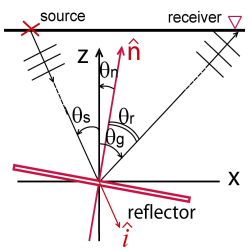

Figure 1, Definition of dip angle and reflection angle

In Figure 1, we define the reflection normal direction as the direction of the bisector of the angle equal θ_s and θ_g. We can transform (θ_s,θ_g) into (θ_n,θ_r) with,

$$\theta_n=(\theta_s+\theta_g)/2$$
$$\theta_r=(\theta_s-\theta_g)/2 \qquad (3)$$

where θ_n is reflector normal

angle to the vertical and θ_r is the reflection angle with respect to the normal. Note that reflector-normal is opposite to the migration-dip in direction, but θ_n is equal to the dip-angle (the angle between X-direction and the dip direction).

Directional Illumination: In order to evaluate the angle domain illumination energy distribution for a given acquisition system with a velocity model, we sum the contributions from all the sources, at the image point, for each angle. That is,

$$D_a(\vec{x},\theta_s)=\sum_s \left| G(s,\vec{x},\theta_s,\omega)\right|^2 \qquad (4)$$

where $D_a(\vec{x},\theta_s)$ is the directional illumination map. DI maps can be used to show the directivity feature of the acquisition illumination.

Acquisition Aperture Efficacy: In order to evaluate the aperture and propagation effects of the given acquisition geometry on energy distribution for a specific area, we use unit impulse as a source at both the source and receiver points for the entire acquisition configuration. Similar to the procedure of DI mapping, we sum up contribution of the Green's functions for each source-receiver pair to get the acquisition aperture efficacy (AAE) matrix, which neglects the detailed wave interface pattern and considers only the energy distribution of the acquisition configuration. That is,

$$E(\vec{x},\theta_n,\theta_r)= \sum_s\{|G(s,\vec{x},\theta_s,\omega)|^2 \sum_r |G(\vec{x},r,\theta_g,\omega)|^2\} \qquad (5)$$

where $E(\vec{x},\theta_n,\theta_r)$ is the AAE matrix at point $\vec{x}$. The value of the AAE matrix at each point indicates how the acquisition aperture and the overlaying structure influence the scattering measurements and imaging process at the point.

Acquisition Dip Response: We can further reduce the acquisition efficacy matrix at each point to a function of reflector dip by summing up all the reflected energy for each reflector. This summation is defined as the acquisition dip response (ADR) of the acquisition geometry. That is,

$$A_d(\vec{x},\theta_n)=\sum_{\theta_r} E(\vec{x},\theta_n,\theta_r) \qquad (6)$$

where $A_d(\vec{x},\theta_n)$ is the ADR vector for point $\vec{x}$. The value of the ADR map measures the dip-angle response of the acquisition system, including the source and receiver apertures.

Implements with one-way and full-wave propagators

For an acquisition geometry on the complex model, the DI, ADR, and AAE are dependent on the type of method used to calculate the Green's function. One of the most accurate numerical methods is the full-wave FD method. But in most cases, the full-wave FD method is not used due to its high computation cost. Instead, one-way wave propagators have been used to implement the illumination analysis, such as GSP, FFD, GDF and LCB beamlet propagator.

Actually, the one-way wave equation is an approximation to the full-wave equation for complex model. Reflection, multiple scattering, and transmission loss which exist in full-wave propagation are neglected in the one-way wave propagation. Furthermore, the numerical methods based on the one-way equation often have inaccurate wide angle amplitudes. One way to estimate these effects is to examine their total effects with numerical methods. Here the LCB beamlet propagator and the space-time domain FD method are employed for the comparison.

The LCB beamlet propagator is a one-way propagator, based on the local reference velocity and local perturbation theory. In this method, the wave fields are windowed and the wave field in beamlet domain is propagated with beamlet propagators.

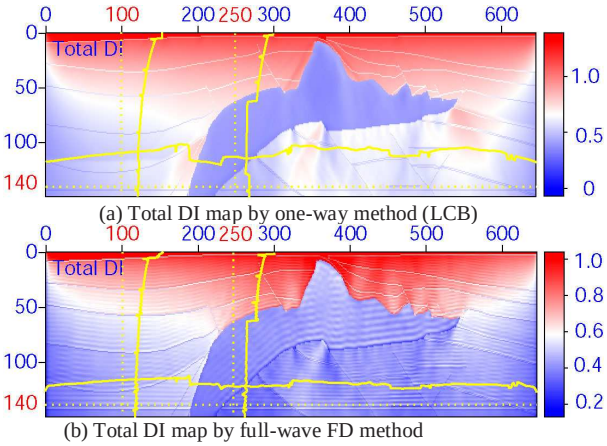

(a) Total DI map by one-way method (LCB)

(b) Total DI map by full-wave FD method

Figure 2, Comparison of the total DI maps by one-way method and full-wave method

Numerical examples

We apply the LCB method and the full-wave FD method to the 2D SEG/EAGE salt model, which has 645 samples with an interval of 80 feet in the horizontal direction and 150 samples with an interval of 80 feet in depth. The minimum velocity is 5000 feet/sec and the maximum velocity is 14700 feet/sec. There are 325 shots with an interval of 160 feet and each shot has 176 receivers in its left-side with an interval of 80feet.

Illumination Comparison: The total illumination maps using the LCB method and the full-wave FD method for the salt model are shown in Figure 2. The total illumination maps from these two methods generally are similar. Illumination amplitude along horizontal line 140, vertical line 100 and 250 are shown in figure 2 (yellow lines). The illumination amplitude varies along horizontal line 140 is similar for both

methods, but slightly larger with the LCB method. For vertical line 250, the illumination amplitude in the subsalt region is weaker for the full wave propagator compared with the one-way method due the strong boundary scattering loss of the full wave propagation, which is neglected in one-way propagation with the LCB method.

ADR Comparison: The total ADR maps by the LCB method and the FD method for the salt model are shown in Figure 3. Similar to the total illumination comparison, the total ADR maps have similar general distribution and some differences in absolute values.

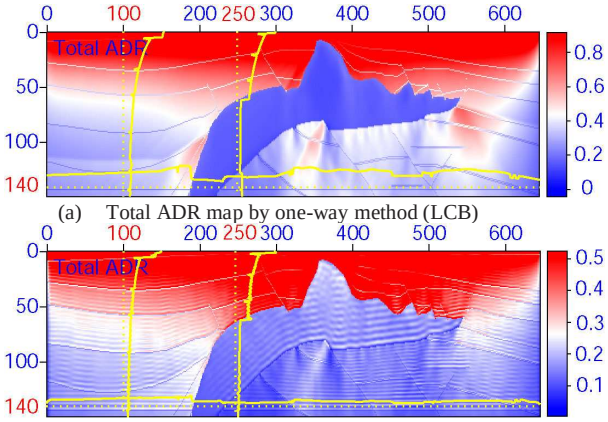

(a) Total ADR map by one-way method (LCB)

(b) Total ADR map by full-wave FD method

Figure 3, Comparison of the total ADR maps by one-way method and full-wave method

The ADR maps for dip angle -40º, 0º and 40º are shown in Figure 4. The maps from the LCB method are shown in Figure 4(a) and those from the full-wave FD method in Figure 4(b). They have similar general distribution. However, the responses in the subsalt area calculated by the full-wave method are weaker than that calculated by the one-way method, again due to the strong scattering loss of the full-wave propagation when across the salt body.

The ADR amplitudes of the two methods along vertical line 250 for all dip-angles are compared in Figure 5. The general distribution is similar but the amplitude with the LCB method decreases with dip angle a little faster than with the FD method.

The ADR amplitudes from the two methods along horizontal line 140 for all dip angles are compared in Figure 6. The general distribution is similar, but the amplitude with the LCB method decreases with dip angle a little faster. This may be caused by the limitation of wide-angle amplitude performance of the one-way propagator.

AAE matrix Comparison: The AAE matrixes for points (100,140), (200,140), (250,140) and (400,140) are shown in Figure 7. The AAE matrixes from the LCB method are shown in Figure 7(a) and those from the FD method, in Figure 7(b). The AAE matrixes for all the points are similar for both methods. But the dip angle and reflection angle response

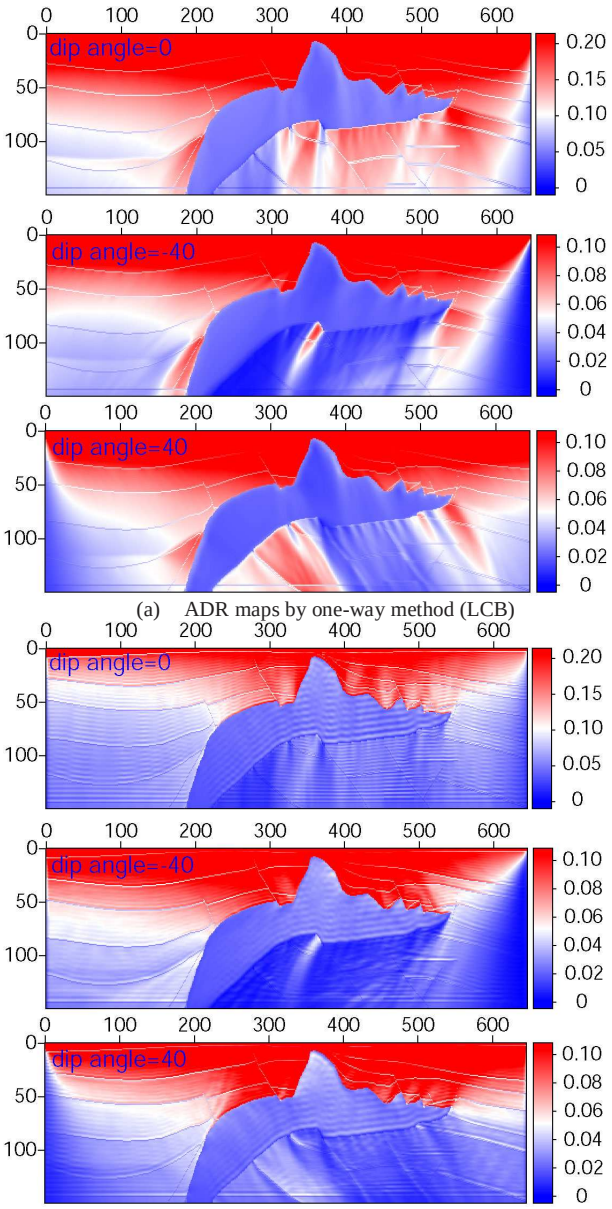

(a) ADR maps by one-way method (LCB)

(b) ADR maps by full-wave FD method

Figure 4, Comparison of the ADR maps for dip angle -40º, 0º and 40º by one-way method and full-wave method

ranges of the FD method are generally larger than those of the LCB method, again due to the difference in wide-angle amplitude responses of the two methods.

Conclusion

The illumination maps from the LCB method and from the FD method have similar general space distributions and angle distributions. Some differences exist especially in the subsalt region. This may be caused by the neglect of scattering loss of the one-way method when passing through the salt body.

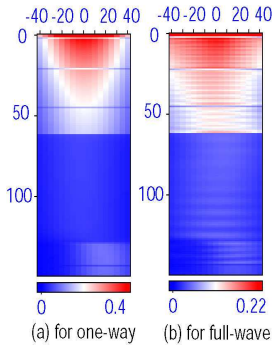

Figure 5, Comparison of the ADR amplitudes along vertical line 250 for all dip angles

Different wide angle amplitude approximation may be attributed to the minor difference in angle span of the two methods. In conclusion, we can use one-way propagators for the estimation of illumination and acquisition aperture response for most of the cases. In some special regions, such as the subsalt area, the strong scattering loss of transmitted waves may need to be taken into consideration if the absolute values of the acquisition responses are needed, such as in the case of amplitude correction. In such cases, the one-way propagator adopted needs to be modified to take into consideration of scattering and reflection loss, intrinsic attenuation loss, etc., for more realistic estimation.

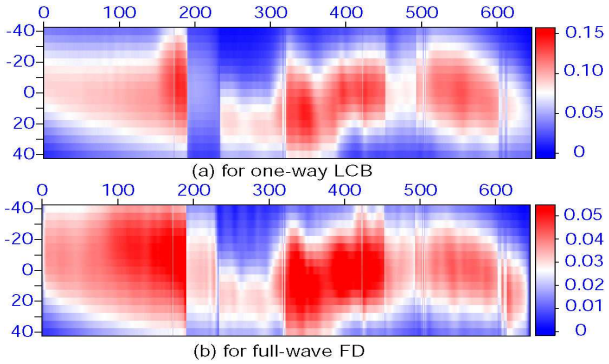

Figure 6, Comparison of the ADR amplitudes along horizontal line 140 for all dip angles.

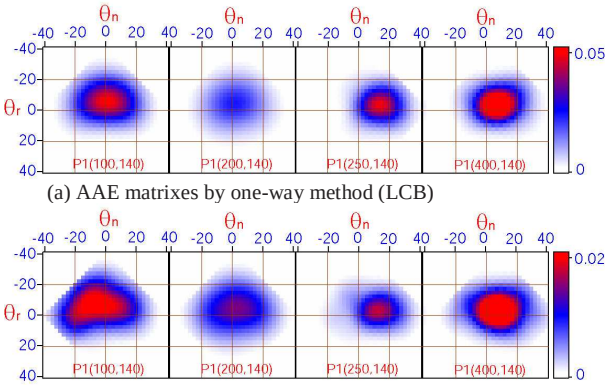

Figure 7, Comparison of the AAE matrix for selected points by one-way method and full-wave method

Acknowledgements:

The authors would like to acknowledge the support from the WTOPI (Wavelet Transform On Propagation and Imaging for seismic exploration) Project and the DOE/Basic Energy Sciences project at University of California, Santa Cruz.

References

Bear, G, LU, C., Lu, R. and Willen, D., 2000, The construction of subsurface illumination and amplitude maps via ray tracing, The Leading Edge, 19(7), 726-728

Berkhout, A.J., 1997, Pushing the limits of seismic imaging, Part I: Prestack migration in terms of double dynamic focusing, Geophysics, 62(3), 937-954.

Hoffmann, 2001, Illumination, resolution and image quality of PP- and PS-waves for survey planning, The Leading Edge, 20(9), 1008-1014.

Luo M. and Wu R.S., 2003, 3D beamlet prestack depth migration using the local cosine basis propagator, Expanded Abstracts, SEG 73th Annual Meeting, 985-988.

Muerdter, D., and Ratcliff, D., 2001a, Understanding subsalt illumination through ray-trace modeling, Part 1: Simple 2D salt models, The Leading Edge, 20(6), 578-594.

Muerdter, D., Kelly, M. and Ratcliff, D., 2001b, Understanding subsalt illumination through ray-trace modeling, Part 2: Dipping salt bodies, salt peaks, and nonreciprocity of subsalt amplitude response, The Leading Edge, 20(7), 688-687.

Muerdter, D., and Ratcliff, D., 2001c, Understanding subsalt illumination through ray-trace modeling, Part 3: Salt ridges and furrows, and impact of acquisition orientation, The Leading Edge, 20(8), 803-816.

Schneider, W.A. and Winbow, G.A., 1999, Efficient and accurate modeling of 3-D seismic illumination, , *Expanded abstracts*, *SEG* 69th Annual Meeting, 633-636

Solid, A. and Ursin, B., 2003, Scattering-angle migration of OBS data in weakly anisotropic media, *Geophysics*, **68**, 641-655

Wang, Y. and Wu, R.S., 2002, Beamlet prestack depth migration using local cosine basis propagator, Expanded Abstracts, SEG 72th Annual Meeting, 1340-1343.

Wu, R.S., Chen, L. and Xie X.B., 2003, Directional illumination and acquisition dip-response, 65th Coference and Technical Exhibition, EAGE, Expanded abstract, P147

Wu, R.S. and Chen, L., 2004, Mapping directional illumination and acquisition dip-response using beamlet propagators, *Geophysics*, accepted.

Wu, R.S., Wang, Y. and Gao, J.H., 2000, Beamlet migration based on local perturbation theory, 70th Ann. Internat. Mtg., Soc. Expl. Geophys., Expanded abstracts, 1008-1011.

Xie, X.B. and Wu, R.S., 2002, Extracting angle related image from migrated wavefield, *Expanded abstracts*, *SEG* 72nd Annual Meeting, 1360-1363.